

Enhanced Hydrogen Evolution Reaction over Co Nanoparticles Embedded N-Doped Carbon Nanotubes Electrocatalyst with Zn as an Accelerant

*Qing Cao, Zhaoyang Cheng, Jiajun Dai, Tianxiao Sun, Guixiang Li, Lili Zhao, Jiayuan Yu, Weijia Zhou, * Jianjian Lin**

Q. Cao, Z. Cheng, Prof. Dr. J. Lin

Key Laboratory of Optic-electric Sensing and Analytical Chemistry for Life Science, MOE, Shandong Key Laboratory of Biochemical Analysis, Qingdao University of Science and Technology, Qingdao, 266042, P. R. China

E-mail: Jianjian_Lin@qust.edu.cn

Dr. L. Zhao, Prof. Dr. J. Yu, Prof. Dr. W. Zhou

Collaborative Innovation Center of Technology and Equipment for Biological Diagnosis and Therapy in Universities of Shandong, Institute for Advanced Interdisciplinary Research (iAIR), University of Jinan, Jinan, 250022, P. R. China

E-mail: ifc_zhouwj@ujn.edu.cn

Q. Cao, J. Dai

Institut für Chemie und Biochemie, Freie Universität Berlin, Arnimallee 22, Berlin, 14195, Germany

Dr. T. Sun, G. Li

Helmholtz-Zentrum Berlin für Materialien und Energie, Hahn-Meitner-Platz 1, Berlin, 14109, Germany

Keywords: carbon nanotubes; Zn, N co-doping; bimetal oxides template; in-situ doping; hydrogen evolution reaction, Zn volatilization

Abstract: The rational design for transition metals-based carbon nano-materials as efficient electrocatalysts still remains a crucial challenge for economical electrochemical hydrogen production. Carbon nanotubes (CNTs) as attractive electrocatalysts are typically activated by non-metal dopant to promote catalytic performance. Metals doping or metal/non-metal

co-doping of CNTs, however, are rarely explored. Herein, we rationally design bimetal oxides template of ZnCo_2O_4 for the heterogeneously doping of Zn and N into Co nanoparticles embedded carbon nanotubes (Co@Zn-N-CNTs). During the formation of CNTs, Zn atoms volatilize from ZnCo_2O_4 and in-situ dope into the carbon skeleton. In particular, owing to the low electronegativity of Zn, the electrons aptly transfer from Zn to carbon atoms, which generates high electron density for the carbon layers and offers more preponderant catalytic sites for hydrogen reduction. The Co@Zn-N-CNTs catalyst exhibits enhanced hydrogen evolution reaction (HER) activity in 0.5 M H_2SO_4 electrolyte, with a low onset potential of -20 mV vs. RHE at 1 mA cm^{-2} , an overpotential of 67 mV at 10 mA cm^{-2} , a small Tafel slope of 52.1 mV dec^{-1} , and persistent long-term stability. This study provides brand-new insights into the utilization of Zn as electronic regulator and activity promoter towards the design of high-efficient electrocatalysts.

1. Introduction

With the excessive exploitation and unscientific use of non-renewable energy sources, such as fossil fuels and coal, the global energy crisis and environmental pollution become more and more serious.^[1] Hydrogen, with the unparalleled superiorities of high energy density and cleanest, is widely regarded as a prospective energy carrier in the future sustainable energy systems.^[2] Among the hydrogen generation strategies, electrochemical water splitting is an environmentally-friendly and economical way for mass production of hydrogen with high purity.^[3] Highly efficient electrochemical catalysts are required to promote hydrogen evolution reaction (HER) with lower overpotential and minimal energy consumption.^[4] To date, platinum (Pt) is still taken for the benchmark for HER catalysts, owing to its near-zero free energy of hydrogen adsorption, the scarcity and soaring cost, however, limits its practical applications.^[5] Hence, the search for comparative electrocatalysts based on non-precious metals and metal-free materials is urgently desired for sustainable large-scale hydrogen production.^[6]

Carbon nanotubes (CNTs), as a typical one-dimensional carbon-based material, have been combined with electrochemically active transition metals (Co, Fe, Ni, *etc.*) to form a complex catalyst,^[7] showing promising electrocatalytic properties for HER.^[8] The conductive carbon supports with unique hollow geometry offer high electrical conductivity, large surface areas and protective shells for transition metals, which make great contributions for improving both the activity and durability of the catalysts.^[9] In addition, doping nonmetallic heteroatoms (N,

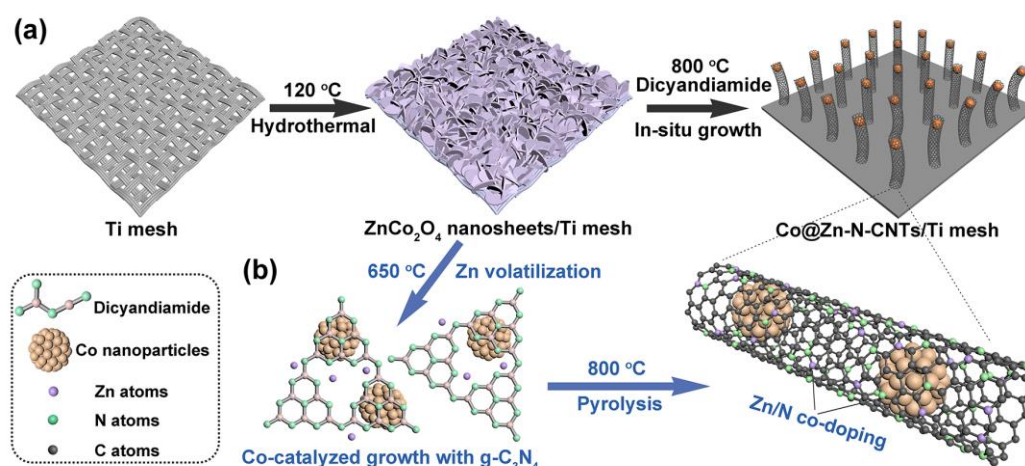
O, B, P, S *etc.*) into the carbon skeleton of CNTs has been emerged as an effective strategy to modify their surface chemistry, adjust electronic structure and thereby improve the catalytic activity.^[10] Nevertheless, transition metal doping or transition metal/non-metal heterogeneous doping of CNTs is rarely reported, where functional doping of CNTs is worth investigating. Bimetallic oxides or hydroxides have been used as ideal templates to introduced the guest metal dopant into the host metal compound. The use of bimetallic templates is also a portable way for the flexible preparation of a series of metal-based (Co, Mo, Ni *etc.*) composite electrocatalysts, such as transition metal carbides^[11] and phosphide^[12]. In addition, the guest metal dopant derived from the bimetal precursor is in-situ introduced without additional metal source, which acts as a promoter to the overall catalytic activity. In view of the current reports, when multiple metals participate in the synthesis of carbon nanotubes, the transition metals are always united with CNTs in the form of nanoparticles,^[9b, 13] bimetal alloy,^[14] transition metal compound (carbide, sulfide, phosphide, nitride *etc.*),^[15] or a mixture of these mentioned structures^[16]. Transition metal doped CNTs electrocatalysts are still of great interest to be explored.

Among most transition metals, Zn element owns both advantages of comparatively low electronegativity (1.66) and stable divalent state, and appears to be a prospective candidate dopant.^[11a, 17] Recently, Zn doping have been designed in the fabrication of electrocatalysts to modulate catalytic activities. On the one hand, Zn doping can modulate the energy level of electrocatalysts to favorable free energy of hydrogen adsorption (near zero) leading to maximum activity towards HER.^[11a, 17a] On the other hand, the low electronegativity of Zn can inject electrons to the atoms with higher electronegativity surrounding them. The atoms accepted additional electrons will generate high electron density which offer more preponderant catalytic sites for hydrogen reduction. For example, different transition metals (Fe, Co, Ni, Cu, and Zn) have been doped into molybdenum sulfide (MoS₂) by a straightforward solvothermal methods. Among all the dopants, Zn-doped MoS₂ catalyst exhibited the lowest onset potential to -0.13 V vs RHE and maximal turnovers of 15.44 s⁻¹ at an overpotential of 300 mV. The Zn dopant not only finely tuned the energy level of MoS₂, but also promoted more active sites through electron injection effect.^[17c]

Over above considerations, here in this work, we rationally design a three-dimensional (3D) electrode of Co nanoparticles encapsulated in Zn-N co-doped carbon nanotubes (Co@Zn-N-CNTs), which is in-situ derived from bimetallic oxides template of ZnCo₂O₄ on Ti mesh. The transition metal Zn and non-metal N are uncommonly heterogeneously introduced into the skeleton of CNTs. Zn, N co-doping can activate carbon atoms to offer more catalytic sites and

adjust the energy level of the electrocatalyst to a favorable free energy of hydrogen adsorption, which is proved by theoretical calculations and X-ray absorption near-edge structure (XANES) spectra. The Co@Zn-N-CNTs exhibits superior electrocatalytic performance towards HER with a low overpotentials of 67 mV at 10 mA cm^{-2} in $0.5 \text{ M H}_2\text{SO}_4$ acidic electrolyte, a small Tafel slope of $50.23 \text{ mV dec}^{-1}$ and good stability. Our results demonstrate that the catalytic activity of Co@Zn-N-CNTs attributes to the coordinated regulation of Co nanoparticles and N, Zn dopant to the CNTs, in which Zn-doping proved to be an effective accelerant. The strategy developed in this work is controllable and can be flexible arranged to introduce binary and even ternary dopant into CNTs with accelerated electrocatalytic performances.

2. Results and discussion



Scheme 1 Schematic illustration showing the (a) fabrication process and (b) mechanism for the formation of Co@Zn-N-CNTs.

As shown in the **Scheme 1a**, the synthesis of Co nanoparticles embedded Zn-N co-doped carbon nanotubes (Co@Zn-N-CNTs) consists two steps. The bimetal Co/Zn oxides template was primarily grown on Ti mesh by a moderate hydrothermal reaction, which were confirmed as ZnCo₂O₄ (JCPDS No. 20-0682) by X-ray diffraction (XRD) characterization (**Figure 1a**). The ZnCo₂O₄ with homogeneous lamellar nanosheets were uniformly oriented on the 3D silks of Ti substrate according to scanning electron microscope (SEM) images (**Figure 1b, c**). The as-formed ZnCo₂O₄ were then subjected to high temperature treatment in an Ar-H₂ atmosphere in the presence of dicyandiamide as carbon and nitrogen source. The formation mechanism of Co@Zn-N-CNTs is illustrated in **Scheme 1b**. At 500 °C-600 °C, the

dicyandiamide can transform into C_3N_4 in gas phase ($g-C_3N_4$),^[13a, 15c] and the CoO nanoparticles can be reduced from $ZnCo_2O_4$ templates by Ar- H_2 atmosphere (**Figure S1** and **S2**). Due to the volatility of Zn above 650 °C,^[11a] the Zn atoms evaporated from $ZnCo_2O_4$ forming pores on the nanosheets (**Figure S3**) and dispersing around the $g-C_3N_4$ (Scheme 1b). With the temperature further increasing to 800 °C, the Co^{2+} nanoparticles easily catalyzed the dissociated C and N decomposed by $g-C_3N_4$ to the in-situ growth of CNTs with N atoms doping.^[13a] At the meantime, the evaporated Zn atoms also participated the formation of carbon skeleton and introduced heteroatomic Zn doping to CNTs. The process was proved by additional contrastive experiment. We synthesized $Co(OH)_2$ nanosheets and ZnO nanorods template by controlling without the adding of Zn salts or Co salts during the synthesis of precursor, respectively. As shown in **Figure S4** and **S5**, the $Co(OH)_2$ nanosheets template transformed into nanotube structures ($Co@N-CNTs$) after carbonization at the same reaction conditions, while the ZnO nanorods precursor remained the rod shape with anomalous carbon shells ($ZnO@C$) (**Figure S6**). It was demonstrable that the CNTs structure was derived from the catalysis of metallic Co in $ZnCo_2O_4$ to the process of carbon dissolution and evolution. The phase composition of $Co@Zn-N-CNTs$ were confirmed by XRD in Figure 1a that the diffraction peaks at 44.52°, 51.58° and 75.87° were attributed to the (111), (200) and (220) crystal faces of metallic Co (JCPDS No. 15-0806), respectively. In addition, the broad diffraction peak at 26.44° was attributed to the (002) face of the graphitized carbon, which was further confirmed by the Raman spectrum (**Figure S7**). The surface morphology of $Co@Zn-N-CNTs$ were characterized by SEM, the prepared $Co@Zn-N-CNTs$ thickly covered the substrate in the interlaced clew shape, which were dozens of microns in length (**Figure 1d, e**). In contrast, the CNTs synthesized from $Co(OH)_2$ nanosheets were only about 2 μm and less uniform in morphology, therefore it was proved that the $ZnCo_2O_4$ template had a better control in morphology during the formation of CNTs (**Figure S4b**).

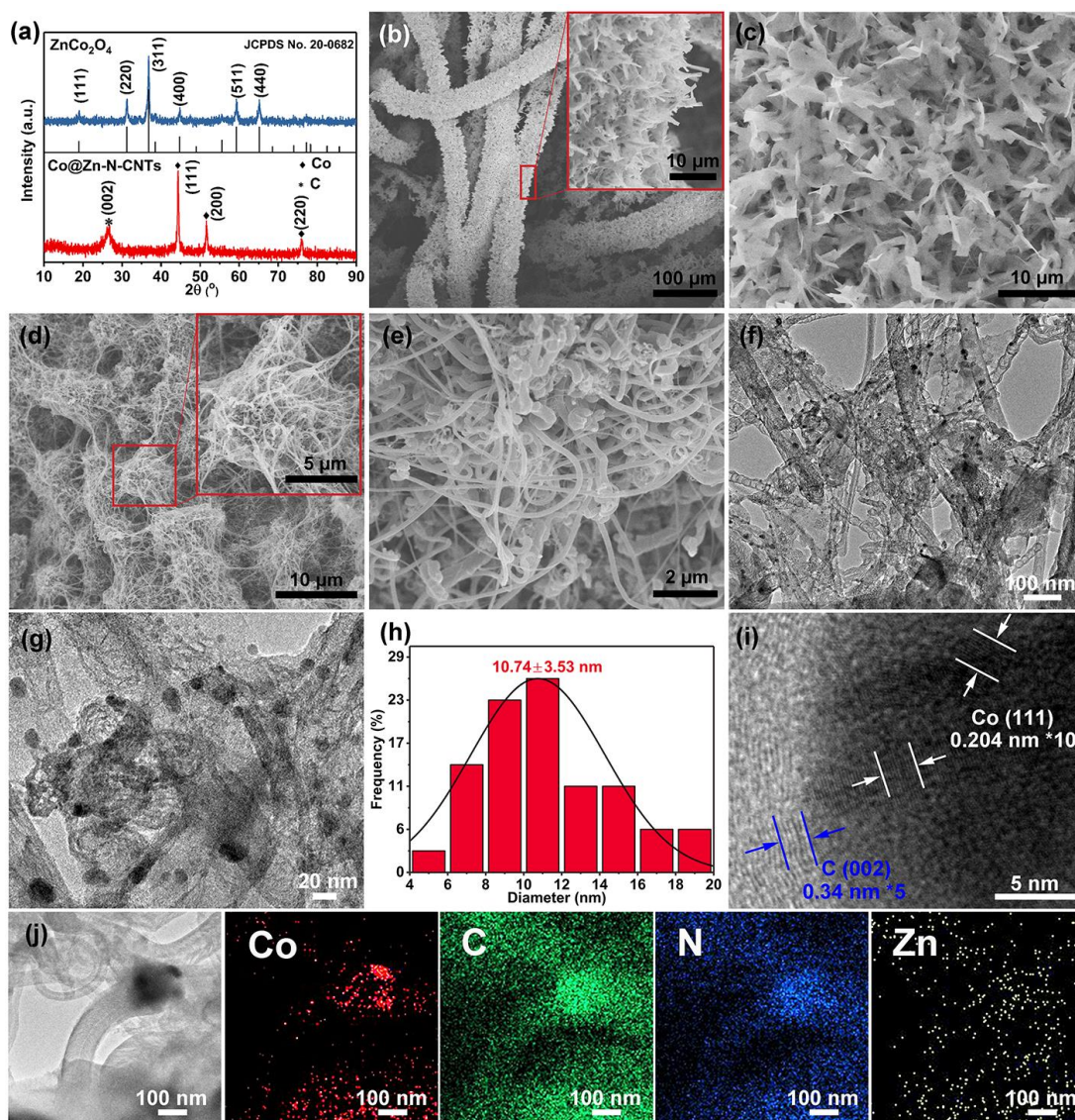


Figure 1 (a) XRD patterns of ZnCo_2O_4 and Co@Zn-N-CNTs . SEM images of (b-c) ZnCo_2O_4 nanosheets and (d-e) Co@Zn-N-CNTs . (f-g) TEM images of Co@Zn-N-CNTs . (h) Statistics of diameters of Co nanoparticles in (g). (i) HRTEM images and (d) EDS mapping of Co@Zn-N-CNTs .

Transmission electron microscopy (TEM) characterizations were carried out to further explore the nanostructure of Co@Zn-N-CNTs . As shown in **Figure 1f**, a mass of metal nanoparticles uniformly embedded in the interlaced carbon nanotubes. From the high magnification TEM image (**Figure 1g**), it was confirmed that the Co nanoparticles with an average diameter of 10.74 ± 3.53 nm (**Figure 1h**) were completely encapsulated by graphene shell. The high-resolution transmission electron microscopy (HRTEM) image (**Figure 1i**) showed that the internal metal nanoparticle displayed a lattice spacing of 0.204 nm, which was matched well with the (111) crystal face of the metal Co. Furthermore, the graphene shell

with a layer thickness of 0.34 nm was corresponding to the (002) crystal face of the C. **Figure 1j** showed the energy dispersive spectroscopy (EDS) characterizations of Co@Zn-N-CNTs. The Co elements were concentrated in the black nanoparticle areas, while the C, N and Zn were homogeneous distributed throughout the whole carbon nanotubes, which verified the core-shell structure of Co@Zn-N-CNTs and N and Zn existed in CNTs by the form of doping. To study the elemental composition and chemical bonding state of ZnCo₂O₄, Co@N-CNTs and Co@Zn-N-CNTs, X-ray photoelectron spectroscopy (XPS) were performed (**Figure 2**). In the C 1s spectrum, the binding energies of 284.5, 285.4, and 287.4 eV were related to C-C, C-N, and C-O bonds respectively in Co@Zn-N-CNTs. Compared to Co@N-CNTs (284.7 eV), the negative shift in binding energies of C-C bonds in Co@Zn-N-CNTs provided the evidence of the electrons transfer from Zn atoms to C atoms. The proportion of C-N bonds in Co@Zn-N-CNTs were higher than in Co@N-CNTs, showing a more favorable N doping concentration (**Figure 2a**). In **Figure 2b**, the peaks observed at 780.1 and 782.0 eV correspond to the Co 2p_{3/2} states and the peaks at 795.5 and 797.6 eV correspond to the Co 2p_{1/2} states in Co@Zn-N-CNTs. The binding energies at 786.4 and 804.3 eV with two shakeup satellites corresponded to oxidized Co arising from superficial oxidation of Co@Zn-N-CNTs due to air contact.^[17a] In **Figure 2c**, the deconvolution peaks of N 1s in Co@Zn-N-CNTs and Co@N-CNTs at 398.2, 399.0 and 401.4 eV corresponded to pyridinic-N, pyrrolic-N and graphitic-N, respectively. The additional peak at 400.6 eV in N 1s spectrum of Co@Zn-N-CNTs was attributable to Zn-N bond owing to the Zn doping.^[18] The binding energies of Zn 2p_{1/2} and Zn 2p_{3/2} appeared at 1022.2 and 1045.3 eV, respectively, suggesting the existence of Zn²⁺ in Co@Zn-N-CNTs (**Figure 2d**). After the high temperature treatment, the content of Zn in Co@Zn-N-CNTs were significant reduced to 0.47 at% compared to 11.99 at% in ZnCo₂O₄, mainly owing to the evaporation of Zn (**Figure 2e**). The content of Co (0.46 at%) and N (6.95 at%) in Co@N-CNTs were much lower than that in Co@Zn-N-CNTs (Co 1.21 at% and N 9.80 at%), while the O content was about 3 times higher, which demonstrated that the bimetal template of ZnCo₂O₄ had a better control during the formation of CNTs for high Co and N proportion (**Figure 2e**).

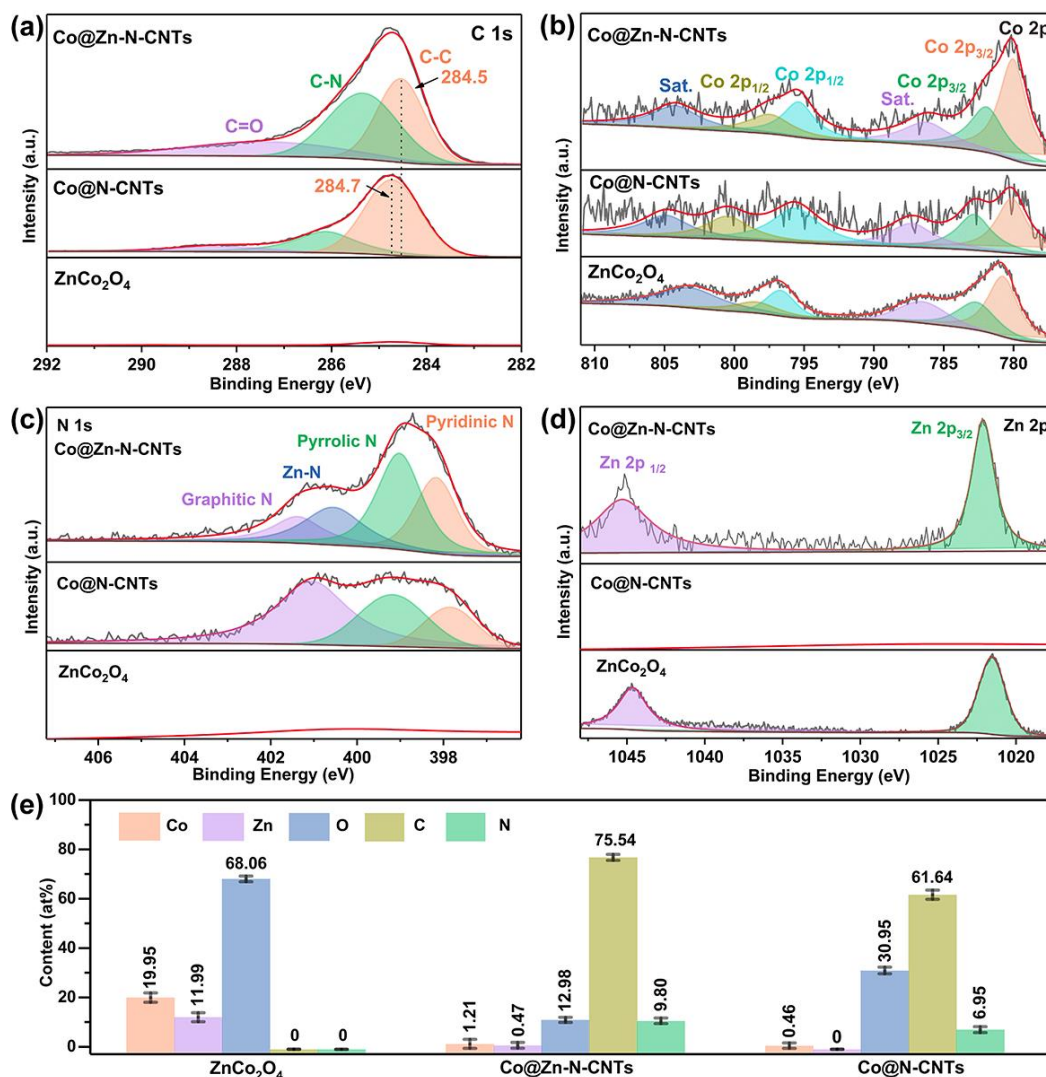


Figure 2 XPS spectra of (a) C 1s, (b) Co 2p, (c) N 1s, and (d) Zn 2p for ZnCo₂O₄, Co@N-CNTs and Co@Zn-N-CNTs. (e) Element contents by XPS analysis.

Scanning transmission X-ray microscopy (STXM) technique coupled with soft X-ray absorption spectroscopy (sXAS) were used to determine the coordination environment and valence state of C and Zn atoms in Co@Zn-N-CNTs. The STXM image of selected measurement area was shown in **Figure S8**. **Figure 3a, c** were the averaged optical density image in C K-edge and Zn L-edge respectively, which indicated the total composition distribution of C and Zn element in the sample. The cluster analysis (CA) is used to classify data in the image stack according to spectral similarities. When searching for clusters, it is looking for pixels with similar weightings of eigenspectra (**Figure 3b** and **S9**). In CA, different clusters mean different material components. The CA of C K-edge shown in **Figure 3b** with 5 coloured areas demonstrated 5 different carbon components in Co@Zn-N-CNTs and the corresponding C K-edge X-ray absorption near-edge structure (XANES) spectra were

shown in **Figure 3e**. The blue colour represented background. Two features at ~ 284.3 eV and 286.0 eV were observed in the π^* region, and these features were attributed to the C=C- and C=N-bonded pyridine structure; the features around 292 eV in the σ^* region were assigned to the C=C and C-N/C=N bond structures.^[19] **Figure 3d** showed the composite mapping of C and Zn in Co@Zn-N-CNTs. Zn was mainly distributed in cluster 1 area in C K-edge (Figure 3b). It can be seen in Figure 3e that the Zn-doped cluster 1 spectrum is broadened towards lower energies than the cluster 2-5 spectra with a negative shift of the C=C bond from 284.5 eV to 284.3 eV, suggesting that the Zn-C bond has been formed and the C atoms most likely acquire electrons from Zn atoms, which consequently resulted in a decrease in the number of C $2P_\pi$ unoccupied states.^[19a] The results also consistent with the XPS characterization in Figure 2a. Compared to Co@N-CNTs, there was a negative shift in binding energies of C-C bonds in Co@Zn-N-CNTs due to Zn doping. STXM based on spatially resolved XAS can provide high spatial resolution imaging and quantitative element analysis over large fields of view, which can reach a more precise results than XPS to the overall element content of the sample. The elements content measured from inductively coupled plasma mass spectrometry (ICP-MS), STXM and average XPS result from 3 different measurement areas were summarized in the **Table S1**. The ICP-MS showed the Co and Zn content in Co@Zn-N-CNTs were 2.35 wt% and 0.47 wt% respectively. The STXM showed that the atomic ratio of C to Zn was 19.8:1. The Zn content measured by STXM were much higher than that by XPS, owing to the limited measurement depth of XPS characterization.

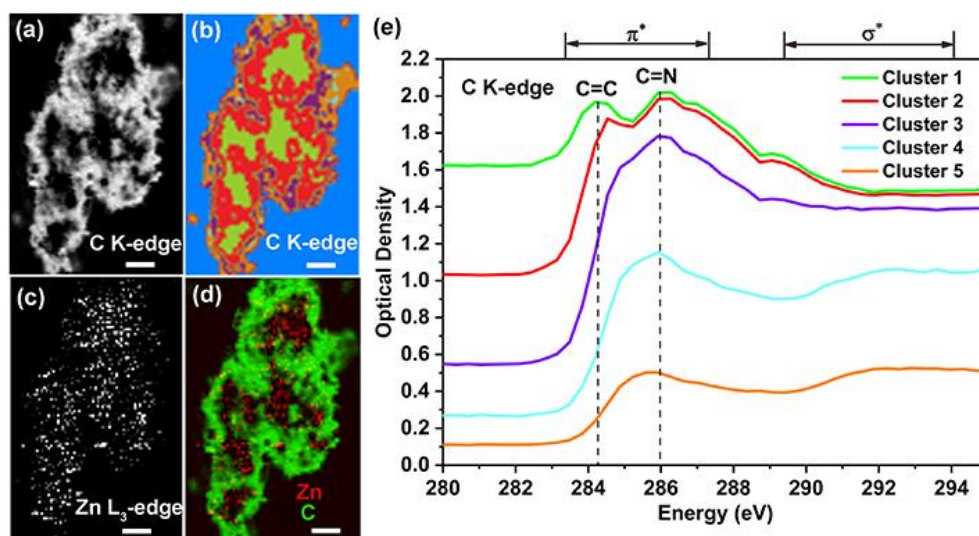


Figure 3 (a) Averaged optical density image and (b) CA in C K-edge. (c) Averaged optical density image in Zn L_3 -edge. (d) Composite mapping of C and Zn in Co@Zn-N-CNTs. The scale bars in (a)-(d) were 2 μm . (e) XANES spectra of C K-edge.

The electrocatalytic activities of Co@Zn-N-CNTs, Co@N-CNTs, ZnO@C, ZnCo₂O₄, Ti mesh and 20 wt% Pt/C were investigated through a three-electrode electrolytic cell system (**Figure S10**). As shown in **Figure 4a**, Co@Zn-N-CNTs exhibited the closest HER activity to 20 wt% Pt/C in all samples, as shown by a partial enlargement of its linear sweep voltammetry (LSV) (**Figure S11**), Co@Zn-N-CNTs had a low onset potential of -20 mV vs. RHE at 1 mA cm⁻² ($\eta_1=20$ mV) and a lower overpotential of 67 mV at 10 mA cm⁻² ($\eta_{10}=67$ mV). It worth noting that the HER performance of Co@Zn-N-CNTs was significantly better than 20 wt% Pt/C at a high current density over 100 mA cm⁻². At a high current density of 300 mA cm⁻², the overpotential of Co@Zn-N-CNTs was only 160 mV, which had a significant advantage over 20 wt% Pt/C working under large current densities. The superior HER activity of Co@Zn-N-CNTs were ascribed to the synergetic modulation of Co nanoparticles, N doping and Zn doping to the carbon atoms and the 3D electrode structure contributed to the large current density.

To emphatically investigate the effect of Zn doping on HER activity, we compared the HER properties of Co@N-CNTs with Co@Zn-N-CNTs. In contrast with Co@Zn-N-CNTs ($\eta_1=20$ mV and $\eta_{10}=67$ mV), Co@N-CNTs had a larger onset potential of -101 mV vs. RHE at 1 mA cm⁻² ($\eta_1=101$ mV) and an overpotential of 184 mV at 10 mA cm⁻² ($\eta_{10}=184$ mV), which revealed that Zn doping played a crucial role in regulating the activity of CNTs. Accordingly, Co@Zn-N-CNTs also showed a small Tafel slope of 50.23 mV dec⁻¹, which was still higher than 20 wt% Pt/C (33.39 mV dec⁻¹) but much lower than Co@N-CNTs (82.34 mV dec⁻¹), indicating that the regulation of Zn doping accelerated the HER kinetics (**Figure 4b**). The HER reaction mechanism of Co@Zn-N-CNTs belonged to Volmer-Heyrovsky mechanism, and the electrochemical desorption process was the rate-limiting step. However, the ZnO@C catalyst showed almost no HER activity and a large Tafel slope over 200 mV dec⁻¹, indicating that Zn had relative inertness as a host of HER catalyst, but significantly activated the carbon shells as a dopant. The ZnCo₂O₄ nanosheets and the pure Ti mesh also had no obvious HER catalytic properties, thereby to eliminate the influence of the substrate during HER performance characterization. In addition, Co@Zn-N-CNTs also exhibited good HER catalytic activities in 1.0 M KOH ($\eta_1=51$ mV and $\eta_{10}=218$ mV) and 1.0 M phosphate buffered saline ($\eta_1=61$ mV and $\eta_{10}=132$ mV) (**Figure S12**). The reasons for the performance improvement by Zn doping are inferred as follows: Firstly, Zn doping can adjust the free energy of hydrogen adsorption of the electrocatalyst to near zero, further increase the HER activity and kinetics.^[11a, 17a] Secondly, it is widely acknowledged that the catalytic active sites

in CNTs are the carbons activated by metal component.^[20] Zn has a low electronegativity (1.66), owing to which electrons tend to transfer from Zn to the surrounding carbon atoms with higher electronegativity. The carbon atoms that accepted additional electrons will generate high electron density which offers more preponderant reactive catalytic sites for the hydrogen reduction.^[17c] This was further proved by the negative shifts in binding energy of C-C bonds in XPS spectrum of Co@Zn-N-CNTs compared to that of Co@N-CNTs. (Figure 2a) A large electrochemically active surface area (ECSA) of the electrode is of great significance to HER, which can both offer a large catalytic surface and more active sites for H₂ evolution. As shown in **Figure 4c** and **S13**, the ECSA of the electrodes were characterized by electric double layer capacitance method. Co@Zn-N-CNTs showed the largest electric double layer capacitance (66.01 mF cm⁻²) than other materials, followed by Co@N-CNTs (63.44 mF cm⁻²). The large ECSA of Co@Zn-N-CNTs was mainly derived from the large specific surface areas of the one-dimensional carbon nanotubes and the co-doping of Zn and N increased the activities of the carbon layers. Raman measurement indicated that the Co@Zn-N-CNTs had a large I_D/I_G of 1.23 (Figure S7). The introduction of Zn and N doping disturbed the sp² bonded carbon network and brought structural defect into CNTs, which generated more active surface area for hydrogen reduction.

We also investigated the electron transfer kinetics of the catalyst by electrochemical impedance spectroscopy (EIS). As shown in **Figure 4d**, we measured the ohmic impedances of Co@Zn-N-CNTs, Co@N-CNTs, ZnO@C, ZnCo₂O₄ and Ti mesh at 300 mV overpotential. Co@Zn-N-CNTs showed significant reduction in the diameter of the semicircle and had the smallest impedance (3.86 Ω), indicating a fast electron transport capability for the hydrogen evolution reaction.

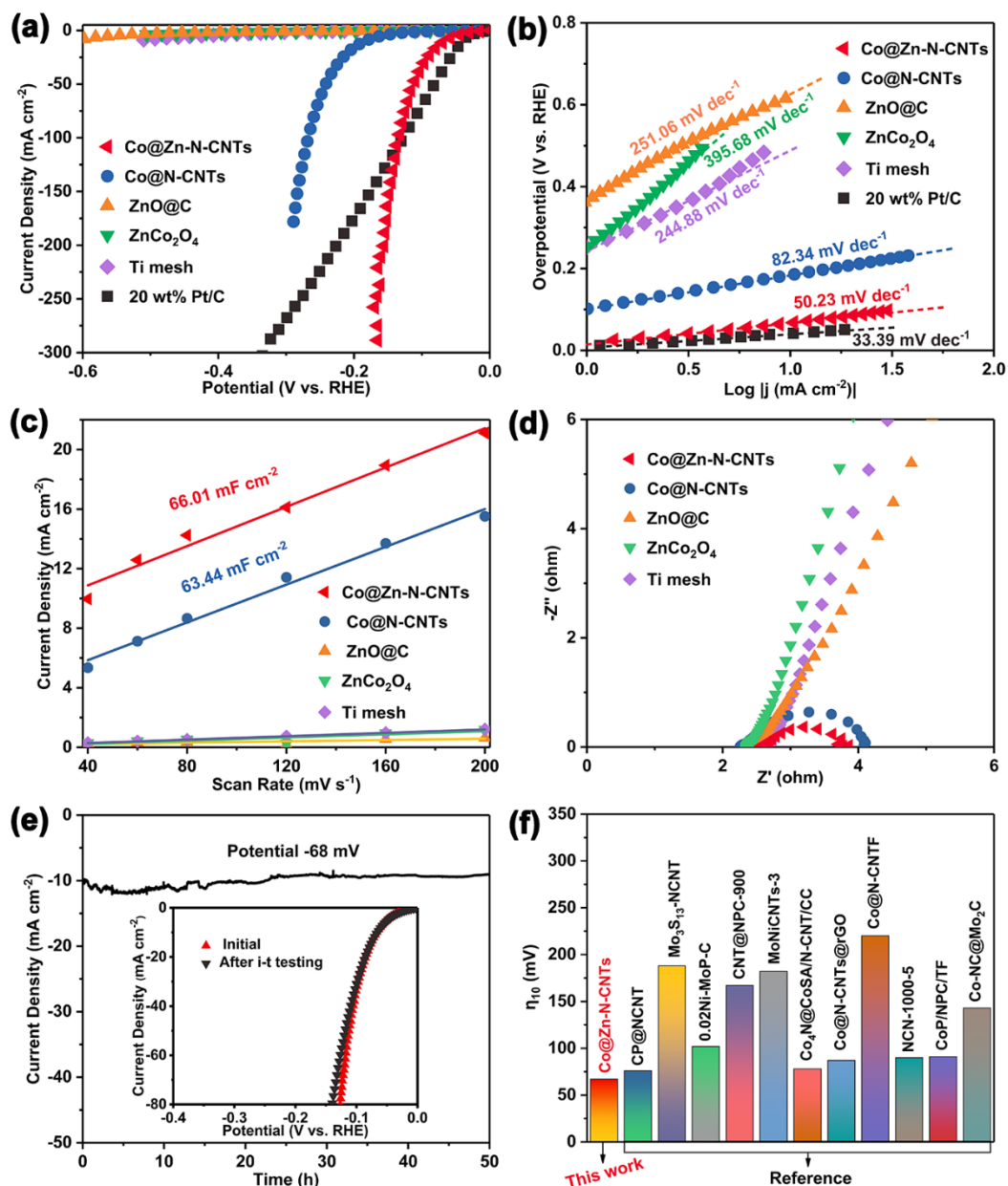


Figure 4 (a) LSV curves and (b) the corresponding Tafel plots of Co@Zn-N-CNTs, Co@N-CNTs, ZnO@C, ZnCo₂O₄, Ti mesh and 20 wt% Pt/C in 0.5 M H₂SO₄. (c) Estimation of double layer capacitance and (d) electrochemical impedance spectra under the overpotential of 300 mV of Co@Zn-N-CNTs, Co@N-CNTs, ZnO@C, ZnCo₂O₄ and Ti mesh. (e) Chronoamperometric response for Co@Zn-N-CNTs at overpotentials of 68 mV for 50 h. Inset of (e) was polarization curves of the Co@Zn-N-CNTs before and after i-t testing. (f) Comparison the activities of Co@Zn-N-CNTs with other recently reported carbon-based HER electrocatalysts in 0.5M H₂SO₄.

Long-term cycle stability is an important criterion for judging the catalytic performance of HER electrocatalysts. We performed a 50-hour i-t test on Co@Zn-N-CNTs at an applied

overpotential of 68 mV to evaluate the stability of Co@Zn-N-C CNTs (**Figure 4e**). Co@Zn-N-CNTs maintained a current density of 10 mA cm⁻² for 50 hours at an overpotential of 68 mV with no significant attenuation. We also compared the polarization curves before and after the i-t test, and the current density was almost no attenuation (inset of Figure 4e). It was confirmed that Co@Zn-N-CNTs had good HER durability in the acidic electrolyte. In addition, the SEM image (**Figure S14**) of Co@Zn-N-CNTs also presented an almost unchanged morphology, verifying the structure stability of Co@Zn-N-CNTs. The metal Co nanoparticles were well protected by carbon nanotubes, so that the structure and properties of the catalyst were well maintained. The Co@Zn-N-CNTs showed a competitive performance comparing to those of recently reported carbon-based HER electrocatalysts^[9c, 15c, 21] in 0.5M H₂SO₄ electrolyte, and the η_{10} of the electrocatalysts are summarized in **Figure 4f** (more detail was shown in **Table S2**).

To unveil the origin of enhancement in intrinsic HER activity, density functional theory (DFT) calculations on the Gibbs free energy of intermediate H* adsorption (ΔG_{H^*} , * represents an adsorption site) and charge density distributions were performed on several models, including pure CNTs (CNTs), N-doped CNTs (N-CNTs), Zn, N-co-doped CNTs (Zn-N-CNTs), Co nanoparticles embedded CNTs (Co@CNTs), Co nanoparticles embedded N-CNTs (Co@N-CNTs) and Co nanoparticles embedded Zn-N-CNTs (Co@Zn-N-CNTs) (**Figure 5a-f**). ΔG_{H^*} is considered a key metric for assessment of HER performance, and a value of ΔG_{H^*} very close to zero is favourable for the H* adsorption and desorption, thus promoting HER.^[14, 21f] As shown in **Figure 5g**, the ΔG_{H^*} of the pure CNTs was +1.57 eV, indicating too weak H* adsorption. After the introduction of N doping and Zn, N co-doping the ΔG_{H^*} were effectively tuned to +0.69 and -0.461 eV respectively. On the other hand, the poor H* adsorption of CNTs also can be improved by the combination with Co nanoparticles, decreasing the ΔG_{H^*} to -0.462 eV. Furthermore, after cooperating the active components of Co nanoparticles with N doping or Zn, N co-doping, the $|\Delta G_{H^*}|$ were further reduced to near zero showing the promotion of HER electrocatalytic activities, which were consistent with the experimental results. And more notably, the calculated ΔG_{H^*} of Co@Zn-N-CNTs displayed different value on different catalytically active sites. When the H* adsorbed on the synergistic site between of Co nanoparticles and the doped Zn atom named as Co@Zn-N-CNTs-S (**Figure 5f**), the $|\Delta G_{H^*}|$ was as low as -0.15 eV, which was much lower than that barely on adjacent Co sites. The synergistic effect of Co nanoparticles and Zn doping exhibited a more favourable H* desorption and leading to faster HER kinetics.

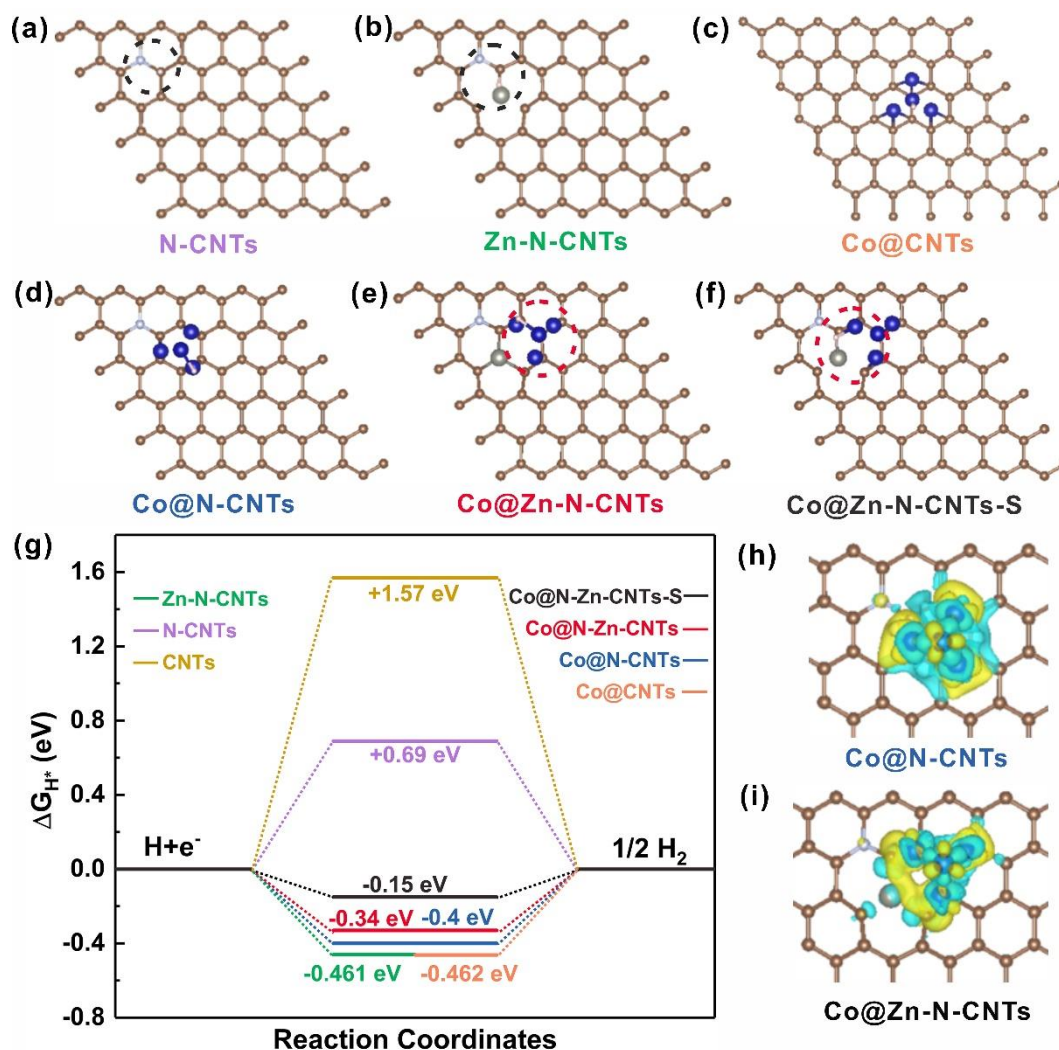


Figure 5 Theoretical analysis of H^* adsorption on models of (a) N-CNTs, (b) Zn-N-CNTs, (c) Co@CNTs, (d) Co@N-CNTs, (e) Co@Zn-N-CNTs (on Co site) and (f) Co@Zn-N-CNTs-S (on Zn, Co synergistic site). C, Co, N, Zn and H are marked in brown, blue, white, gray and pink respectively. (g) The calculated free-energy diagram of the HER on CNTs, N-CNTs, Zn-N-CNTs, Co@CNTs, Co@N-CNTs, Co@Zn-N-CNTs and Co@Zn-N-CNTs-S. (h) Charge density differences in the catalyst models of (h) Co@N-CNTs and (i) Co@Zn-N-CNTs. Yellow and cyan represent charge accumulation and depletion, respectively.

Subsequently, to further clarify the tuning mechanism from the electronic state, charge density differences between C layer, Co nanoparticles, N doping and Zn doping in different models were analysed (**Figure 5h, i** and **Figure S15**). As shown in **Figure S15a**, when doping with the strong electron acceptor of atomic N (CNTs), the electrons in the C layer were transferred to the N atom, leading to the reduction of charge densities of C layer. On the contrary, the introduction of Zn atom obviously changed the charge densities in the N-CNTs

(Figure S15b). The electrons were transferred from Zn atom to C and N atoms, generating the increase of the overall electron densities in the surrounding C regions, which was in good agreement with the XPS and STXM results (Figure 2a and Figure 3). Similarly, the loading of Co nanoparticles also induced distinct C rich regions through the charge transfer from Co to C (Figure S15c), altering the π -conjugated system of C and creating the in-plane charge polarization in the C layer.^[9b] Furthermore, as shown in Figure 5i, the cooperation of strong electron donor Co and atomic Zn with low electronegativity led to strong electronic coupling in Co@Zn-N-CNTs. Particularly, the C regions between Co nanoparticles and doped Zn atom showed intense electron aggregation, owing to the synergetic electron transfer of Co and Zn to C layer. It was also in accordance with the calculation results of ΔG_{H^*} . The electron-rich Co@Zn-N-CNTs-S showed the low-desorption energy of H^* in the HER.^[15c, 22] Additionally, the combination of N dopant to the model of Co@N-CNTs and Co@Zn-N-CNTs rebalanced the charge densities of the system (Figure 5h, i) and adjusted the adsorption ability to H^* , thus enhanced the HER activity. Therefore, the engineering of Co-C conjugation and Zn, N co-doping can effectually optimize the electrocatalytic performance.

3. Conclusion

In summary, benefitting from the metallic oxides template of $ZnCo_2O_4$, the transition metal Zn was successfully in-situ doped into the synthesis of CNTs with a controllable morphology and catalytic favorable high Co, N content. In this work, the Co@Zn-N-CNTs exhibited the highest activity with an overpotential of only 67 mV at 10 mA cm^{-2} and a low Tafel slope of $50.23 \text{ mV dec}^{-1}$ in 0.5 M H_2SO_4 . The superior HER activity of Co@Zn-N-CNTs was ascribed to the synergetic modulation of Co nanoparticles and Zn, N co-doping. DFT calculations and STXM-XANES characterization proved that Zn doping adjusted the electronic structures of Co@Zn-N-CNTs by transferring electrons to C and reduced the free energy of hydrogen adsorption of the electrocatalyst. The 3D electrode structure contributed to the large current density of Co@Zn-N-CNTs and the HER property was significantly better than 20 wt% Pt/C at a high current density over 100 mA cm^{-2} . This study not only offers us an efficient 3D catalyst for the production of hydrogen fuel, but also opens an attractive avenue to explore transition metal Zn as an accelerant and modulator towards high-efficient catalysis and other applications.

4. Experimental Section

Materials: All chemicals used in this study were of analytical grade and used without further purification. Zinc nitrate hexahydrate ($\text{Zn}(\text{NO}_3)_2 \cdot 6\text{H}_2\text{O}$) was bought from Tianjin Damao Chemical Reagent Factory (China). Cobaltous nitrate hexahydrate ($\text{Co}(\text{NO}_3)_2 \cdot 6\text{H}_2\text{O}$) urea ($\text{CO}(\text{NH}_2)_2$) and ammonium hydrogen fluoride (NH_4F) were purchased from Shanghai Aladdin Bio-Chem Technology Co., LTD (China). Dicyandiamide ($\text{C}_2\text{H}_4\text{N}_4$), sulfuric acid (H_2SO_4), sodium dihydrogen phosphate ($\text{NaH}_2\text{PO}_4 \cdot 2\text{H}_2\text{O}$), sodium phosphate dibasic dehydrate ($\text{Na}_2\text{HPO}_4 \cdot 7\text{H}_2\text{O}$) and nafion solution (~5%, a mixture of lower aliphatic alcohols and water) were purchased from Shanghai Macklin Biochemical Co., Ltd (China). 20 wt% Pt/C was purchased from Sinopharm Chemical Reagents Beijing Co., Ltd (China). Hydrochloric acid (HCl) and ethanol ($\text{CH}_3\text{CH}_2\text{OH}$) were purchased from Guangzhou Chemical Reagent Factory (China). Ti mesh (1000 meshes) was bought from Oufulang Metal Wire Mesh Manufacturing Co., Ltd (China). Argon and hydrogen gas mixture (Ar–H₂, 10 vol% H₂) and hydrogen (H₂) were bought from Guangzhou YIGAS Gases Co., Ltd (China). Deionized water (DI-water) was supplied with a Barnstead Nanopure Water System (18.3 M Ω cm) and was used throughout this experiment.

Preparation of ZnCo_2O_4 nanosheets, ZnO nanorods and $\text{Co}(\text{OH})_2$ nanowires on Ti mesh: The Ti mesh substrate with an area of $3 \times 2 \text{ cm}^2$ was pretreated by ultrasonically washing with 1M HCl solution, ethanol and DI water several times to remove surface impurities and metal passivated layer, followed by drying for use.

Through a typical hydrothermal preparation process, 0.09 g $\text{Zn}(\text{NO}_3)_2 \cdot 6\text{H}_2\text{O}$, 0.18 g $\text{Co}(\text{NO}_3)_2 \cdot 6\text{H}_2\text{O}$, 0.75 g $\text{CO}(\text{NH}_2)_2$ and 0.19 g NH_4F were dissolved in 35 mL deionized water under magnetic stirring. The pretreated Ti mesh was first placed in a 50 mL Teflon-lined stainless-steel autoclave with the above mixed solution transferred into and heated at 120 °C for 5 hours. After the autoclave was naturally cooled to room temperature, the Ti mesh grown with pink product was taken out and washed several times with DI water and absolute ethanol, and dried in an oven at 60 °C overnight.

The ZnO nanorods and $\text{Co}(\text{OH})_2$ nanowires were prepared through the same hydrothermal method with controlled additives. The ZnO nanorods and $\text{Co}(\text{OH})_2$ nanowire were obtained by without adding $\text{Co}(\text{NO}_3)_2 \cdot 6\text{H}_2\text{O}$ and $\text{Zn}(\text{NO}_3)_2 \cdot 6\text{H}_2\text{O}$ respectively, and the remaining steps were unchanged.

Preparation of Co@Zn-N-CNTs , ZnO@C and Co@N-CNTs on Ti mesh: The former prepared Ti mesh loaded with ZnCo_2O_4 nanosheets was cut into an area of $1 \times 1.5 \text{ cm}^2$ and put in a ceramic crucible which was placed in the center of a quartz tube inside a tubular furnace with 1000 mg $\text{C}_2\text{H}_4\text{N}_4$ placed in front. The tubular furnace was quickly heated from ambient

temperature to 800 °C with a heating rate of 5 °C min⁻¹ and maintained at 800 °C for 2 h under an Ar–H₂ (9:1) flow at a flow rate of 50 sccm. After calcination, the surface of the Ti mesh became black and the Co@Zn-N-CNTs were synthesized. The Co@Zn-N-CNTs were washed with 1M HCl and DI water to remove the Co nanoparticles that are not protected by carbon.

Similarly, the ZnO nanorods covered by carbon shell (ZnO@C) and Co nanoparticles embedded in N-doped carbon nanotubes (Co@N-CNTs) were synthesized by the same way using ZnO nanorods and Co(OH)₂ nanowires as precursors respectively to study the HER catalytic performance of Zn and the influence of Zn doping.

Supporting Information

Supporting Information is available from the Wiley Online Library or from the author.

Acknowledgements

Q. Cao and Z. Cheng contributed equally to this work. The authors acknowledge financial support from the Young Taishan Scholarship Project of Shandong Province (J. Lin: tsqn201909115; W. Zhou: tsqn201812083). The North-German Supercomputing Alliance (HLRN) is acknowledged for computer time. Prof. Dr. Beate Paulus from Freie Universität Berlin is acknowledged for the modification of DFT calculations.

Received: ((will be filled in by the editorial staff))

Revised: ((will be filled in by the editorial staff))

Published online: ((will be filled in by the editorial staff))

References

- [1] a) M. S. Dresselhaus, I. L. Thomas, *Nature* **2001**, *414*, 332-337; b) J. A. Turner, *Science* **2004**, *305*, 972-974.
- [2] a) J. Zhang, Q. Zhang, X. Feng, *Adv. Mater.* **2019**, *31*, 1808167; b) W. Lubitz, W. Tumas, *Chem. Rev.* **2007**, *107*, 3900-3903.
- [3] P. J. McHugh, A. D. Stergiou, M. D. Symes, *Adv. Energy Mater.* **2020**, *10*, 2002453.

- [4] a) I. Roger, M. A. Shipman, M. D. Symes, *Nat. Rev. Chem.* **2017**, *1*, 0003; b) T. Qiu, Z. Liang, W. Guo, S. Gao, C. Qu, H. Tabassum, H. Zhang, B. Zhu, R. Zou, Y. Shao-Horn, *Nano Energy* **2019**, *58*, 1-10.
- [5] M. Q. Yang, J. Wang, H. Wu, G. W. Ho, *Small* **2018**, *14*, 1703323.
- [6] a) L. Li, P. Wang, Q. Shao, X. Huang, *Chem. Soc. Rev.* **2020**, *49*, 3072-3106; b) D. Strmcnik, P. P. Lopes, B. Genorio, V. R. Stamenkovic, N. M. Markovic, *Nano Energy* **2016**, *29*, 29-36; c) T. Wang, H. Xie, M. Chen, A. D'Aloia, J. Cho, G. Wu, Q. Li, *Nano Energy* **2017**, *42*, 69-89; d) L. Li, Z. Deng, L. Yu, Z. Lin, W. Wang, G. Yang, *Nano Energy* **2016**, *27*, 103-113; e) C. Pi, Z. Zhao, X. Zhang, B. Gao, Y. Zheng, P. K. Chu, L. Yang, K. Huo, *Chem. Eng. J.* **2021**, *416*, 129130; f) Y.-Z. Wang, Y.-M. Ding, C.-H. Zhang, B.-W. Xue, N.-W. Li, L. Yu, *Rare Met.* **2021**, *40*, 2785-2792.
- [7] a) J. Feng, H. C. Zeng, *J. Phys. Chem. B* **2005**, *109*, 17113-17119; b) J. Deng, P. Ren, D. Deng, L. Yu, F. Yang, X. Bao, *Energy Environ. Sci.* **2014**, *7*, 1919-1923; c) N. S. Kim, Y. T. Lee, J. Park, J. B. Han, Y. S. Choi, S. Y. Choi, J. Choo, G. H. Lee, *J. Phys. Chem. B* **2003**, *107*, 9249-9255; d) Y. Qin, S. M. Lee, A. Pan, U. Gosele, M. Knez, *Nano Lett.* **2008**, *8*, 114-118; e) D. D. Chronopoulos, H. Saini, I. Tantis, R. Zboril, K. Jayaramulu, M. Otyepka, *Small* **2022**, *18*, e2104628; f) R. Sharma, E. Moore, P. Rez, M. M. Treacy, *Nano Lett.* **2009**, *9*, 689-694; g) Y. Liu, H. Jiang, Y. Zhu, X. Yang, C. Li, *J. Mater. Chem. A* **2016**, *4*, 1694-1701; h) L. Xia, X. Zhang, H. Song, Y. Zheng, X. Li, B. Gao, K. Huo, P. K. Chu, *Int. J. Hydrog. Energy* **2020**, *45*, 22629-22637.
- [8] a) W. J. Zhou, J. Jia, J. Lu, L. J. Yang, D. M. Hou, G. Q. Li, S. W. Chen, *Nano Energy* **2016**, *28*, 29-43; b) D. Voiry, H. S. Shin, K. P. Loh, M. Chhowalla, *Nat. Rev. Chem.* **2018**, *2*, 1-17.
- [9] a) D. H. Kweon, M. S. Okyay, S. J. Kim, J. P. Jeon, H. J. Noh, N. Park, J. Mahmood, J. B. Baek, *Nat. Commun.* **2020**, *11*, 1278; b) Z. Chen, R. Wu, Y. Liu, Y. Ha, Y. Guo, D. Sun, M. Liu, F. Fang, *Adv. Mater.* **2018**, *30*, 1802011; c) H. Guo, Q. Feng, J. Zhu, J. Xu, Q. Li, S. Liu, K. Xu, C. Zhang, T. Liu, *J. Mater. Chem. A* **2019**, *7*, 3664-3672.
- [10] a) L. H. Zhang, Y. Shi, Y. Wang, N. R. Shiju, *Adv. Sci.* **2020**, *7*, 1902126; b) Z. Wang, S. Zhang, X. Lv, J. Bai, W. Yu, J. Liu, *Int. J. Hydrog. Energy* **2019**, *44*, 16478-16486; c) J. Wang, F. Xu, H. Jin, Y. Chen, Y. Wang, *Adv. Mater.* **2017**, *29*, 1605838; d) D. W. Wang, D. S. Su, *Energy Environ. Sci.* **2014**, *7*, 576-591; e) Y.-G. Zhu, C.-Q. Shang, Z.-Y. Wang, J.-Q. Zhang, M.-Y. Yang, H. Cheng, Z.-G. Lu, *Rare Met.* **2019**, *40*, 90-95.

- [11] a) Q. Cao, L. Zhao, A. Wang, L. Yang, L. Lai, Z. L. Wang, J. Kim, W. Zhou, Y. Yamauchi, J. Lin, *Nanoscale* **2019**, *11*, 1700-1709; b) L. Zhao, H. Yuan, D. Sun, J. Jia, J. Yu, X. Zhang, X. Liu, H. Liu, W. Zhou, *Nano Energy* **2020**, *77*, 105056.
- [12] a) T. Liu, X. Ma, D. Liu, S. Hao, G. Du, Y. Ma, A. M. Asiri, X. Sun, L. Chen, *ACS Catal.* **2016**, *7*, 98-102; b) Y. Zhang, Y. Liu, M. Ma, X. Ren, Z. Liu, G. Du, A. M. Asiri, X. Sun, *Commun. Chem.* **2017**, *53*, 11048-11051; c) C. Tang, R. Zhang, W. Lu, L. He, X. Jiang, A. M. Asiri, X. Sun, *Adv. Mater.* **2017**, *29*, 1602441.
- [13] a) X. Zou, X. Huang, A. Goswami, R. Silva, B. R. Sathe, E. Mikmeková, T. Asefa, *Angew. Chem. Int. Ed.* **2014**, *126*, 4461-4465; b) X. Zhou, X. Liu, J. Zhang, C. Zhang, S. J. Yoo, J.-G. Kim, X. Chu, C. Song, P. Wang, Z. Zhao, D. Li, W. Zhang, W. Zheng, *Carbon* **2020**, *166*, 284-290; c) N. Cheng, N. Wang, L. Ren, G. Casillas-Garcia, N. Liu, Y. Liu, X. Xu, W. Hao, S. X. Dou, Y. Du, *Carbon* **2020**, *163*, 178-185.
- [14] J. Deng, P. Ren, D. Deng, L. Yu, F. Yang, X. Bao, *Energy Environ. Sci.* **2014**, *7*, 1919-1923.
- [15] a) Z. Ye, J. Yang, B. Li, L. Shi, H. Ji, L. Song, H. Xu, *Small* **2017**, *13*, 1700111; b) Q. Liu, J. Tian, W. Cui, P. Jiang, N. Cheng, A. M. Asiri, X. Sun, *Angew. Chem. Int. Ed.* **2014**, *53*, 6710-6714; c) B. Cao, M. Hu, Y. Cheng, P. Jing, B. Liu, B. Zhou, X. Wang, R. Gao, X. Sun, Y. Du, J. Zhang, *NPG Asia Mater.* **2021**, *13*, 1-14; d) W. Zhou, J. Lu, K. Zhou, L. Yang, Y. Ke, Z. Tang, S. Chen, *Nano Energy* **2016**, *28*, 143-150.
- [16] a) T. Ouyang, Y. Q. Ye, C. Y. Wu, K. Xiao, Z. Q. Liu, *Angew. Chem. Int. Ed.* **2019**, *58*, 4923-4928; b) S. Gao, Y. Zhang, Y. Zhang, B. Wang, S. Yang, *Small* **2018**, *14*, 1804388; c) Y. Guo, P. Yuan, J. Zhang, H. Xia, F. Cheng, M. Zhou, J. Li, Y. Qiao, S. Mu, Q. Xu, *Adv. Func. Mater.* **2018**, *28*, 1805641.
- [17] a) T. Liu, D. Liu, F. Qu, D. Wang, L. Zhang, R. Ge, S. Hao, Y. Ma, G. Du, A. M. Asiri, L. Chen, X. Sun, *Adv. Energy Mater.* **2017**, *7*, 1700020; b) Z. Cai, A. Wu, H. Yan, C. Tian, D. Guo, H. Fu, *Energy Technol.* **2019**, *8*, 1901079; c) Y. Shi, Y. Zhou, D. R. Yang, W. X. Xu, C. Wang, F. B. Wang, J. J. Xu, X. H. Xia, H. Y. Chen, *J. Am. Chem. Soc.* **2017**, *139*, 15479-15485; d) Q. Yang, C. C. Yang, C. H. Lin, H. L. Jiang, *Angew. Chem. Int. Ed.* **2019**, *58*, 3511-3515.
- [18] L. Han, S. Song, M. Liu, S. Yao, Z. Liang, H. Cheng, Z. Ren, W. Liu, R. Lin, G. Qi, X. Liu, Q. Wu, J. Luo, H. L. Xin, *J. Am. Chem. Soc.* **2020**, *142*, 12563-12567.
- [19] a) S. C. Ray, C. W. Pao, J. W. Chiou, H. M. Tsai, J. C. Jan, W. F. Pong, R. McCann, S. S. Roy, P. Papakonstantinou, J. A. McLaughlin, *J. Appl. Phys.* **2005**, *98*, 033708; b) S. C. Ray, C. W. Pao, H. M. Tsai, J. W. Chiou, W. F. Pong, C. W. Chen, M. H. Tsai,

- P. Papakonstantinou, L. C. Chen, K. H. Chen, W. G. Graham, *Appl. Phys. Lett.* **2007**, *90*, 192107.
- [20] a) C. Huang, D. Wu, P. Qin, K. Ding, C. Pi, Q. Ruan, H. Song, B. Gao, H. Chen, P. K. Chu, *Nano Energy* **2020**, *73*, 104788; b) H. Lei, Z. Wang, F. Yang, X. Huang, J. Liu, Y. Liang, J. Xie, M. S. Javed, X. Lu, S. Tan, W. Mai, *Nano Energy* **2020**, *68*, 104293.
- [21] a) D. Yang, W. Hou, Y. Lu, W. Zhang, Y. Chen, *J. Energy Chem.* **2021**, *52*, 130-138; b) P. K. R. Holzapfel, M. Buhler, D. Escalera-Lopez, M. Bierling, F. D. Speck, K. J. J. Mayrhofer, S. Cherevko, C. V. Pham, S. Thiele, *Small* **2020**, *16*, 2003161; c) W. Xiao, L. Zhang, D. Bukhvalov, Z. Chen, Z. Zou, L. Shang, X. Yang, D. Yan, F. Han, T. Zhang, *Nano Energy* **2020**, *70*, 104445; d) F. Xiao, Z. Chen, H. Wu, Y. Wang, E. Cao, X. Lu, Y. Wu, Z. Ren, *Nanoscale* **2019**, *11*, 23027-23034; e) X. Zhang, P. Yang, S. P. Jiang, *Carbon* **2021**, *175*, 176-186; f) Z. Chen, R. Wu, Y. Liu, Y. Ha, Y. Guo, D. Sun, M. Liu, F. Fang, *Adv. Mater.* **2018**, *30*, 1802011; g) H. Jiang, J. Gu, X. Zheng, M. Liu, X. Qiu, L. Wang, W. Li, Z. Chen, X. Ji, J. Li, *Energy Environ. Sci.* **2019**, *12*, 322-333; h) X. Huang, X. Xu, C. Li, D. Wu, D. Cheng, D. Cao, *Adv. Energy Mater.* **2019**, *9*, 1803970; i) Q. Liang, H. Jin, Z. Wang, Y. Xiong, S. Yuan, X. Zeng, D. He, S. Mu, *Nano Energy* **2019**, *57*, 746-752.
- [22] a) X. Han, X. Wu, Y. Deng, J. Liu, J. Lu, C. Zhong, W. Hu, *Adv. Energy Mater.* **2018**, *8*, 1800935; b) R. Gao, L. Pan, H. Wang, X. Zhang, L. Wang, J.-J. Zou, *ACS Catal.* **2018**, *8*, 8420-8429.

Zn atoms volatilize from ZnCo_2O_4 and in-situ co-dope with N atoms into the carbon skeleton during the formation of carbon nanotubes. The Zn-doped carbon nanotubes have a more controllable morphology and catalytic favorable high Co, N content, showing better HER activity than 20 wt% Pt/C over 100 mA cm^{-2} . Zn doping is an effective accelerant to the HER electrocatalytic activity.

*Qing Cao, Zhaoyang Cheng, Jiajun Dai, Tianxiao Sun, Guixiang Li, Lili Zhao, Jiayuan Yu, Weijia Zhou, * Jianjian Lin**

Enhanced Hydrogen Evolution Reaction over Co Nanoparticles Embedded N-Doped Carbon Nanotubes Electrocatalyst with Zn as an Accelerant

